

# Carbon–Carbon Bond Fragmentation in Aminoalcohol Radical Cations. Kinetics, Thermodynamic Correlations, and Mechanism

Richard D. Burton, Michael D. Bartberger, Yin Zhang, John R. Eyler, and Kirk S. Schanze\*

Contribution from the Department of Chemistry, University of Florida, P.O. Box 117200, Gainesville, Florida 32611

Received February 5, 1996<sup>⊗</sup>

**Abstract:** A detailed study of the kinetics, thermodynamics and mechanism of carbon–carbon bond fragmentation in a series of aminoalcohol radical cations is presented. The compounds that provide the basis for this investigation are derived from the parent structure, *erythro*-2-(phenylamino)-1,2-diphenylethanol, by substitution at the *para* position of the *N*-phenyl with methoxy, methyl, (hydrogen), chloro, and cyano groups (compounds **1a–e**, respectively). The rates for C–C bond fragmentation for radical cations **1a–e**<sup>+</sup> in CH<sub>3</sub>CN solution were determined by laser flash photolysis and vary from  $3.9 \times 10^4$  (**1a**) to  $7.4 \times 10^6$  s<sup>-1</sup> (**1e**). The activation parameters for bond fragmentation in **1c–e**<sup>+</sup> are characterized by low activation enthalpies and relatively large, negative activation entropies. The bond fragmentation rates increase with the peak potential for anodic oxidation of the neutral aminoalcohols,  $E_p(\mathbf{1})$ . Correlation of the free energy of activation for bond fragmentation ( $\Delta G_{\text{BF}}^\ddagger$ ) with  $FE_p(\mathbf{1})$  ( $F$  is the Faraday constant) implies that the dependence of  $\Delta G_{\text{BF}}^\ddagger$  on  $\Delta G^\circ_{\text{BF}}$  is relatively weak, consistent with bond fragmentation in **1a–e**<sup>+</sup> being weakly endothermic or exothermic. The transient absorption spectra of the reactive intermediates produced by fragmentation of **1a–e**<sup>+</sup> are consistent with a mechanism involving heterolytic fragmentation of the C<sub>1</sub>–C<sub>2</sub> bond with concomitant loss of the hydroxyl proton. By contrast, FT-ICR studies of **1a–e**<sup>+</sup> indicate that in the gas phase homolytic fragmentation of the C<sub>1</sub>–C<sub>2</sub> bond predominates. Semiempirical calculations using the AM1 Hamiltonian demonstrate that in the gas phase homolysis is the thermodynamically preferred pathway, consistent with the FT-ICR results.

## Introduction

Radical ions are important reactive intermediates in single electron transfer (SET) chemistry.<sup>1</sup> Given the importance of SET chemistry to chemical synthesis and mechanism, there has been a recent upsurge of research activity focused on understanding the unique reactivity of organic radical cations and radical anions.<sup>2–13</sup> These studies have led to new synthetic methodologies<sup>3e,f,4</sup> and provided a unique opportunity to understand bonding in odd-electron species.<sup>6,9,10</sup> Furthermore, research on radical ions is beginning to provide a basis for

understanding the thermodynamic<sup>6,14,15</sup> and kinetic origins of the significantly enhanced reactivity of these reactive intermediates.

Radical ions are the primary reactive intermediates produced by photoinduced electron transfer.<sup>16,17</sup> The reactivity of these high-energy intermediates affords the means to apply photo-

<sup>⊗</sup> Abstract published in *Advance ACS Abstracts*, June 1, 1996.

(1) For recent reviews in the area of SET chemistry see: *Advances in Electron Transfer Chemistry*; Mariano, P. S., Ed.; JAI Press: Greenwich; 1991–1994; Vols. 1–4.

(2) Chanon, M.; Rajzmann, M.; Chanon, F. *Tetrahedron* **1990**, *46*, 6193.

(3) (a) Arnold, D. R.; Maroulis, A. J. *J. Am. Chem. Soc.* **1976**, *98*, 5931. (b) Popielarz, R.; Arnold, D. R. *J. Am. Chem. Soc.* **1990**, *112*, 3068. (c) Nicholas, A. M.; Arnold, D. R. *Can. J. Chem.* **1982**, *60*, 2165. (d) Nicholas, A. M.; Boyd, R. J.; Arnold, D. R. *Can. J. Chem.* **1982**, *60*, 3011. (e) McMahon, K.; Arnold, D. R. *Can. J. Chem.* **1993**, *71*, 450. (f) Arnold, D. R.; Du, X. *Can. J. Chem.* **1994**, *72*, 403.

(4) (a) Eitsu, H.; Xu, W.; Mariano, P. S. *J. Am. Chem. Soc.* **1988**, *110*, 8099. (b) Jeon, Y. T.; Lee, C.-P.; Mariano, P. S. *J. Am. Chem. Soc.* **1991**, *113*, 8847. (c) Xu, W.; Zhang, X.-M.; Mariano, P. S. *J. Am. Chem. Soc.* **1991**, *113*, 8863. (d) Yoon, U. C.; Mariano, P. S. *Acc. Chem. Res.* **1992**, *25*, 233. (e) Zhang, X.; Yeh, S.-R.; Hong, S.; Freccero, M.; Albini, A.; Falvey, D. E.; Mariano, P. S. *J. Am. Chem. Soc.* **1994**, *116*, 4211.

(5) (a) Workentin, M. S.; Johnston, L. J.; Parker, V. D. *J. Am. Chem. Soc.* **1994**, *116*, 8279. (b) Workentin, M. S.; Schepp, N. P.; Johnston, L. J. *J. Am. Chem. Soc.* **1994**, *116*, 1141. (c) Johnston, L. J.; Kwong, P.; Shelemay, A. *J. Am. Chem. Soc.* **1993**, *115*, 1664.

(6) (a) Maslak, P. In *Photoinduced Electron Transfer V. Top. Curr. Chem.* **1993**, *168*, 1. (b) Maslak, P. **1990**, *29*, 283. (c) Maslak, P.; Chapman, W. H., Jr.; Vallombroso, T. M.; Watson, B. M. *J. Am. Chem. Soc.* **1995**, *117*, 12380. (d) Maslak, P.; Vallombroso, T. M.; Chapman, W. H., Jr.; Narvaez, J. N. *Angew. Chem., Int. Ed. Engl.* **1994**, *33*, 73.

(7) (a) Dinnocenzo, J. P.; Banach, T. E. *J. Am. Chem. Soc.* **1989**, *111*, 8646. (b) Dinnocenzo, J. P.; Conlon, J. P. *Tetrahedron Lett.* **1995**, *36*, 7415. (c) Dinnocenzo, J. P.; Karki, S. B.; Jones, J. P. *J. Am. Chem. Soc.* **1993**, *115*, 7111. (d) Karki, S. B.; Dinnocenzo, J. P.; Jones, J. P.; Korzekwa, K. R. *J. Am. Chem. Soc.* **1995**, *117*, 3657.

(8) (a) Mirafzal, G. A.; Kim, T.; Liu, J.; Bauld, N. L. *J. Am. Chem. Soc.* **1992**, *114*, 10968. (b) Yueh, W.; Bauld, N. L. *J. Am. Chem. Soc.* **1995**, *117*, 5671. (c) Yueh, W.; Bauld, N. L. *J. Chem. Soc., Perkins Trans. 2* **1995**, 871. (d) Bellville, D. J.; Pabon, R. A.; Bauld, N. L. *J. Am. Chem. Soc.* **1985**, *107*, 4978.

(9) (a) Roth, H. D.; Herberz, T. *J. Am. Chem. Soc.* **1993**, *115*, 9801. (b) Ishiguro, K.; Turro, N. J.; Roth, H. D. *J. Am. Chem. Soc.* **1994**, *116*, 6933. (c) Weng, X.; Du, X.-M.; Roth, H. D. *J. Am. Chem. Soc.* **1995**, *117*, 135. (d) Weng, X.; Sheik, Q.; Roth, H. D. *J. Am. Chem. Soc.* **1995**, *117*, 10655.

(10) (a) Schlessener, C. J.; Amatore, C.; Kochi, J. K. *J. Am. Chem. Soc.* **1984**, *106*, 7472. (b) Masnovi, J. M.; Sankararaman, S.; Kochi, J. K. *J. Am. Chem. Soc.* **1989**, *111*, 2263. (c) Sankararaman, S.; Perrier, S.; Kochi, J. K. *J. Am. Chem. Soc.* **1989**, *111*, 6448. (d) Perrier, S.; Sankararaman, S.; Kochi, J. K. *J. Chem. Soc., Perkin Trans. 2* **1993**, 825.

(11) (a) Reitstöen, B.; Parker, V. D. *J. Am. Chem. Soc.* **1990**, *112*, 4968. (b) Parker, V. D.; Chao, Y.; Reitstöen, B. *J. Am. Chem. Soc.* **1991**, *113*, 2336. (c) Parker, V. D.; Tilset, M. *J. Am. Chem. Soc.* **1991**, *113*, 8778.

(12) Horner, J. H.; Martinez, F. N.; Musa, O. M.; Newcomb, M.; Shahin, H. E. *J. Am. Chem. Soc.* **1995**, *117*, 11124.

(13) Baciocchi, E.; Del Giacco, T.; Elisei, F. *J. Am. Chem. Soc.* **1993**, *115*, 12290.

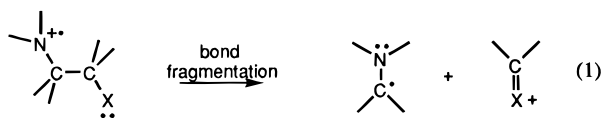
(14) (a) Zhang, X.-M.; Bordwell, F. G.; Satish, A. V. *Pure Appl. Chem.* **1995**, *67*, 735. (b) Bordwell, F. G.; Zhang, X.-M.; Cheng, J.-P. *J. Org. Chem.* **1993**, *58*, 6410. (c) Bordwell, F. G.; Satish, A. V. *J. Am. Chem. Soc.* **1992**, *114*, 10173. (d) Bordwell, F. G.; Harrelson, J. A., Jr.; Satish, A. V. *J. Org. Chem.* **1989**, *54*, 3101. (e) Bordwell, F. G.; Cheng, J.-P. *J. Am. Chem. Soc.* **1989**, *111*, 1792.

(15) Wayner, D. D. M.; Parker, V. D. *Acc. Chem. Res.* **1993**, *26*, 287.

chemistry, and more specifically photoinduced electron transfer, to drive energetically uphill processes in chemical synthesis and energy conversion.<sup>16,17</sup> Furthermore, knowledge of the rates of specific radical ion reactions such as deprotonation,<sup>7a,10a,11,13</sup> carbon-carbon<sup>6,10c,d</sup> and carbon-heteroatom<sup>4,5c</sup> bond scission, rearrangements,<sup>9</sup> and addition to unsaturated bonds<sup>8a,12</sup> provides a method to probe the dynamics of geminate ion-radical pairs born in the primary event of photoinduced electron transfer.

Amine radical cations have been the focus of much work in radical ion chemistry. Early photochemical and electrochemical work suggested that the acidity of protons on a carbon that is  $\alpha$  to an amine radical cation is greatly enhanced relative to the corresponding neutral amines.<sup>18-20</sup> More recent studies by Lewis,<sup>21</sup> von Sonntag,<sup>22</sup> Dinnocenzo,<sup>7</sup> Parker,<sup>11c</sup> and Mariano<sup>4e</sup> provide a quantitative thermodynamic and kinetic description of this effect. Studies also reveal that the departure of a variety of electrofugal groups is significantly enhanced by an  $\alpha$ -amine radical cation center.<sup>4</sup>

Our interest has centered on the reactivity of radical cations derived from 2-aminoalcohols and 1,2-diamines.<sup>23</sup> These radical cations undergo facile C-C bond fragmentation in a manner consistent with the expectation that the amine radical cation activates the adjacent C-C  $\sigma$  bond, e.g.,



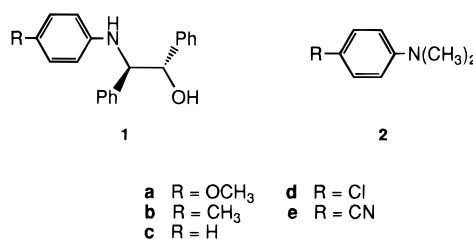
X = OH : aminoalcohol

X = NR<sub>2</sub> : diamine

Whitten's work along with our own indicated that the dynamics of C-C bond fragmentation depend on a variety of factors including the structure of the electrofugal group, the stereochemistry, and the relative stability of the radical cation as reflected by the oxidation potential of the neutral amine.<sup>23,24</sup>

The objective of the present study was to determine the relationship between the dynamics of C-C bond scission and

the relative stability of the radical cation for the series of structurally related 2-aminoalcohols, **1a-e**. The peak potentials for irreversible oxidation of the neutral aminoalcohols were determined by electrochemistry, while the rates and activation parameters for C-C bond fragmentation of the radical cations **1a-e**<sup>•+</sup> were determined by laser flash photolysis. The results of this study indicate that there is a strong correlation between the free energy of activation for C-C bond fragmentation and the peak potential for anodic oxidation of the aminoalcohol. Furthermore, comparison of the reaction in CH<sub>3</sub>CN solution and in the gas phase reveals interesting features concerning the mechanism of the C-C bond fragmentation process.



## Experimental Section

**Materials.** Solvents and chemicals used for synthesis were of reagent grade and used without purification unless noted. Silica gel (Merck, 230-400 mesh) was used for chromatography. NMR spectra were obtained on a GE QE 300-MHz spectrometer. Metal complex *fac*-[(bpy)Re<sup>I</sup>(CO)<sub>3</sub>(4-benzylpyridine)<sup>+</sup>][PF<sub>6</sub><sup>-</sup>] (**3**) was synthesized and characterized as described previously.<sup>25a</sup>

**erythro-2-[(*p*-Methoxyphenyl)amino]-1,2-diphenylethanol (1a).** *p*-Anisidine (1.25 g, 10.2 mmol) was added to a Schlenk tube which was subsequently placed under argon. Then 50 mL of dry CH<sub>2</sub>Cl<sub>2</sub> was added to the Schlenk tube via a cannula. The Schlenk tube was cooled to 0 °C on an ice-water bath whereupon 5.7 mL of a 2.0 M solution of Al(CH<sub>3</sub>)<sub>3</sub> in hexane (11.4 mM) was added via a syringe. The solution was stirred for 1 h after which time 2.0 g of *trans*-stilbene oxide (10.2 mmol) dissolved in 5 mL of CH<sub>2</sub>Cl<sub>2</sub> was slowly added. The reaction was monitored by TLC (silica gel, 35% hexanes/CH<sub>2</sub>Cl<sub>2</sub>); a spot at *R*<sub>f</sub> = 0.35 was observed after 45 min. After 2 h, the *trans*-stilbene oxide spot at *R*<sub>f</sub> ≈ 0.9 had disappeared and the reaction was quenched by addition of 5% aqueous NaOH. The solution was extracted with two 25-mL portions of CH<sub>2</sub>Cl<sub>2</sub>. The combined organic fractions were dried over MgSO<sub>4</sub>, and the solvent was then removed under reduced pressure to yield 1 g of a brownish oily solid. The crude product was purified by flash chromatography (silica gel, 25% ethyl acetate/hexanes). Pure **1a** was obtained as a white crystalline solid, 0.5 g (yield 15%). NMR analysis confirmed that the sample contains less than 5% of the *threo* isomer.

Spectral data: TLC (silica, 35% hexanes/CH<sub>2</sub>Cl<sub>2</sub>) *R*<sub>f</sub> = 0.35; <sup>1</sup>H NMR (300 MHz, CDCl<sub>3</sub>)  $\delta$  3.69 (s, 3H), 4.62 (d, *J* = 4.6 Hz, 1H), 5.07 (d, *J* = 4.6 Hz, 1H), 7.00-7.31 (m, 14H); <sup>13</sup>C NMR (75 MHz, CDCl<sub>3</sub>)  $\delta$  55.7, 64.7, 77.1, 114.8, 115.5, 126.6, 127.3, 127.9, 128.1, 128.2, 138.8, 140.1, 140.9, 152.5. Anal. Calcd for C<sub>21</sub>H<sub>21</sub>NO<sub>2</sub>: C, 78.95; H, 6.64; N, 4.38. Found: C, 78.76; H, 6.63; N, 4.30.

**erythro-2-[(*p*-Methylphenyl)amino]-1,2-diphenylethanol (1b).** This compound was synthesized following the procedure outlined for **1a**, except that 1.64 g of *p*-toluidine (15.3 mmol) was used in place of *p*-anisidine. The amounts of the other reagents were scaled-up accordingly.

After extraction, 1.0 g of crude **1b** was obtained as a white solid. The crude material was purified by recrystallization from EtOH/H<sub>2</sub>O (1:1 v/v). The purified product was obtained as white crystals, yield 750 mg (16%). NMR analysis confirmed that the product contained less than 5% of the *threo* isomer.

Spectral data: TLC (silica, 35% hexanes/CH<sub>2</sub>Cl<sub>2</sub>) *R*<sub>f</sub> = 0.35; <sup>1</sup>H NMR (300 MHz, CDCl<sub>3</sub>)  $\delta$  2.25 (s, 3H), 2.48 (s, 1H), 4.67 (d, *J* = 4.5 Hz, 1H), 5.09 (d, *J* = 4.5 Hz, 1H), 7.15-7.30 (m, 14H); <sup>13</sup>C NMR (75

(25) (a) Wang, Y.; Schanze, K. S. *Inorg. Chem.* **1994**, *33*, 1354. (b) Wang, Y.; Schanze, K. S. *Chem. Phys.* **1993**, *176*, 305.

(16) For an excellent series of reviews of photoinduced electron transfer and the reactivity of radical ions derived therefrom see: (a) *Photoinduced Electron Transfer*, Fox, M. A., Chanon, M. D., Eds.; Elsevier: Amsterdam, 1988; Parts A-D. (b) *Photoinduced Electron Transfer I*. In *Top. Curr. Chem.* **1990**, *156*, 1-125. (c) *Photoinduced Electron Transfer III*. In *Top. Curr. Chem.* **1991**, *159*, 1-259. (d) *Photoinduced Electron Transfer IV*. In *Top. Curr. Chem.* **1992**, *163*, 1-245. (e) *Photoinduced Electron Transfer V*. In *Top. Curr. Chem.* **1993**, *168*, 1-270.

(17) (a) Mattes, S. L.; Farid, S. *Science* **1984**, *226*, 917. (b) Gould, I. R.; Ege, D.; Moser, J. E.; Farid, S. *J. Am. Chem. Soc.* **1990**, *112*, 4290. (c) Gould, I. R.; Moser, J. E.; Armitage, B.; Farid, S. *Res. Chem. Intermed.* **1995**, *21*, 793.

(18) Cohen, S. G.; Parola, A.; Parsons, G. H. *Chem. Rev.* **1973**, *73*, 141.

(19) Peters, K. S.; Schaeffer, C. G. *J. Am. Chem. Soc.* **1980**, *102*, 7566.

(20) Mann, C. K.; Barnes, K. K. *Electrochemical Reactions in Non-Aqueous Systems*; Marcel Dekker: New York, 1970.

(21) (a) Lewis, F. D. *Acc. Chem. Res.* **1986**, *19*, 401. (b) Lewis, F. D. *Adv. Photochem.* **1986**, *13*, 165. (c) Lewis, F. D.; Bassani, D. M.; Burch, E. L.; Cohen, B. E.; Engleman, J. A.; Reddy, G. D.; Schneider, S.; Jaeger, W.; Gedeck, P.; Gahr, M. *J. Am. Chem. Soc.* **1995**, *117*, 660.

(22) Das, S.; von Sonntag, C. *Z. Naturforsch.* **1986**, *41b*, 505.

(23) (a) Wang, Y.; Hauser, B. T.; Rooney, M. M.; Burton, R. D.; Schanze, K. S. *J. Am. Chem. Soc.* **1993**, *115*, 5675. (b) Lucia, L. A.; Burton, R. D.; Schanze, K. S. *J. Phys. Chem.* **1993**, *97*, 9078. (c) Wang, Y.; Lucia, L. A.; Schanze, K. S. *J. Phys. Chem.* **1995**, *99*, 1961. (d) Lucia, L. A.; Wang, Y.; Nafisi, K.; Netzel, T. L.; Schanze, K. S. *J. Phys. Chem.* **1995**, *99*, 11801. (e) Wang, Y.; Schanze, K. S. *J. Phys. Chem.*, in press.

(24) (a) Ci, X.; Lee, L. Y. C.; Whitten, D. G. *J. Am. Chem. Soc.* **1987**, *109*, 2536. (b) Kellett, M. A.; Whitten, D. G. *J. Am. Chem. Soc.* **1989**, *111*, 2314. (c) Ci, X.; Whitten, D. G. *J. Am. Chem. Soc.* **1989**, *111*, 3459. (d) Bergmark, W. R.; Whitten, D. G. *J. Am. Chem. Soc.* **1990**, *112*, 4042. (e) Ci, X.; Kellett, M. A.; Whitten, D. G. *J. Am. Chem. Soc.* **1991**, *113*, 3893. (f) Leon, J. W.; Whitten, D. G. *J. Am. Chem. Soc.* **1993**, *115*, 8038. (g) Gan, H.; Leinhos, U.; Gould, I. R.; Whitten, D. G. *J. Am. Chem. Soc.* **1995**, *99*, 3566.

MHz, CDCl<sub>3</sub>)  $\delta$  20.3, 64.1, 77.1, 114.2, 126.6, 127.2, 127.5, 127.9, 128.2, 129.6, 138.7, 140.1, 144.5. Anal. Calcd for C<sub>21</sub>H<sub>21</sub>NO: C, 83.12; H, 6.99; N, 4.62. Found: C, 83.17; H, 7.01; N, 4.55.

**erythro-2-(Phenylamino)-1,2-diphenylethanol (1c).** This compound was synthesized following the procedure outlined for **1a**, except that 1.64 g of aniline (18.0 mmol) was used in place of *p*-anisidine. The amounts of the other reagents were scaled-up accordingly.

After extraction, 1.5 g of crude **1c** was obtained as a yellow solid. The crude material was purified by recrystallization from EtOH/H<sub>2</sub>O (1:1 v/v). The purified product was obtained as white crystals, yield 1.05 g (20%). NMR analysis confirmed that the product contained less than 5% of the *threo* isomer.

Spectral data: TLC (silica, 35% hexanes/CH<sub>2</sub>Cl<sub>2</sub>)  $R_f$  = 0.25; <sup>1</sup>H NMR (300 MHz, CDCl<sub>3</sub>)  $\delta$  2.48 (s, 1H, amino), 4.70 (d,  $J$  = 4.5 Hz, 1H), 5.11 (d,  $J$  = 4.5 Hz, 1H), 7.08–7.31 (m, 15H); <sup>13</sup>C NMR (75 MHz, CDCl<sub>3</sub>)  $\delta$  63.8, 77.2, 114.0, 118.0, 126.5, 127.6, 128.0, 128.2, 129.1, 138.5, 140.1, 146.8. Anal. Calcd for C<sub>20</sub>H<sub>19</sub>NO: C, 83.01; H, 6.62; N, 4.84. Found: C, 82.91; H, 6.66; N, 4.74.

**erythro-2-[(*p*-Chlorophenyl)amino]-1,2-diphenylethanol (1d).** *p*-Chloroaniline (3.2 g, 25 mmol) and *trans*-stilbene oxide (1.0 g, 5.1 mmol) were ground up together by using a mortar and pestle. The chloroaniline/stilbene oxide mixture and a magnetic stir bar were placed into a heavy-walled glass tube that was fitted with a Teflon high-vacuum stopcock. The tube was evacuated under high vacuum and then sealed by closing the stopper. The tube was heated to 150 °C in a sand bath while the mixture was stirred by using a magnetic stirring motor. (This temperature was sufficient to melt the mixture.) The tube was cooled at intervals of 24 h and the reaction mixture was analyzed by TLC (silica gel, 35% hexanes/CH<sub>2</sub>Cl<sub>2</sub>). After 4 days the *trans*-stilbene oxide spot at  $R_f$  = 0.9 had disappeared and at this point the reaction was deemed complete. The crude reaction product was dissolved in CH<sub>2</sub>Cl<sub>2</sub> and filtered and then the solvent was removed under reduced pressure. The resulting crude product was a yellowish-brown solid which was purified by recrystallization two times from ethyl acetate/hexanes (4:1 v/v). The recrystallized product was obtained as a powdery white solid, yield 700 mg (43% based on *trans*-stilbene oxide). NMR analysis confirmed that the product contained less than 1% of the *threo* isomer.

Spectral data: <sup>1</sup>H NMR (300 MHz, CDCl<sub>3</sub>)  $\delta$  2.35 (s, 1H, amino), 4.70 (d,  $J$  = 4.5 Hz, 1H, methine adjacent to hydroxyl), 5.18 (d,  $J$  = 4.5 Hz, 1H, methine adjacent to amino), 7.02–7.38 (m, 14H, phenyls); <sup>13</sup>C NMR (75 MHz, CDCl<sub>3</sub>)  $\delta$  63.9 (adjacent to hydroxyl), 77.2 (adjacent to amino), 115.0, 126.5, 127.7, 127.9, 128.1, 128.3, 128.9, 138.1, 139.9, 145.4 (all aromatic) Anal. Calcd for C<sub>20</sub>H<sub>18</sub>ClNO: C, 74.17; H, 5.61; N, 4.33. Found: C, 74.34; H, 5.67; N, 4.25.

**erythro-2-[(*p*-Cyanophenyl)amino]-1,2-diphenylethanol (1e).** *p*-Aminobenzonitrile (2.41 g, 20.4 mmol) and *trans*-stilbene oxide (2.0 g, 10.2 mmol) were ground up together by using a mortar and pestle. The aminobenzonitrile/stilbene oxide mixture and a magnetic stir bar were placed into a heavy-walled glass tube that was fitted with a Teflon high-vacuum stopcock. The tube was evacuated under high vacuum and then sealed by closing the stopper. The tube was heated to 150 °C in a sand bath while the mixture was stirred by using a magnetic stirring motor. (This temperature was sufficient to melt the mixture.) The reaction was monitored by TLC (25% ethyl acetate/hexanes); a new spot at  $R_f$  = 0.20 was observed after 2 h. The reaction was allowed to proceed for 14 h until it appeared that the *trans*-stilbene oxide spot at  $R_f$  = 0.9 had disappeared. The brownish mixture was cooled to room temperature after which time the resulting solid was dissolved in CH<sub>2</sub>Cl<sub>2</sub>. The solution was filtered and dried over MgSO<sub>4</sub> and the solvent was removed under reduced pressure. The resulting crude product was purified by recrystallization two times from ethyl acetate/hexanes (4:1 v/v). The recrystallized product was obtained as a powdery white solid, yield 750 mg (23% based on *trans*-stilbene oxide). NMR analysis confirmed that the product contained less than 1% of the *threo* isomer.

Spectral data: TLC (silica, 25% hexanes/CH<sub>2</sub>Cl<sub>2</sub>)  $R_f$  = 0.20. <sup>1</sup>H NMR (300 MHz, CDCl<sub>3</sub>)  $\delta$  2.49 (s, 1H), 4.68 (d,  $J$  = 4.5 Hz, 1H), 5.15 (d,  $J$  = 4.5 Hz, 1H), 7.05–7.45 (m, 14H); <sup>13</sup>C NMR (75 MHz, CDCl<sub>3</sub>)  $\delta$  62.5, 75.4, 120.9, 96.4, 113.2, 127.2, 127.4, 127.8, 128.0, 128.8, 133.5, 140.2, 143.4, 151.5. Anal. Calcd for C<sub>21</sub>H<sub>18</sub>N<sub>2</sub>O: C, 80.22; H, 5.78; N, 8.91. Found: C, 80.48; H, 5.89; N, 8.83.

## Methods and Equipment for Photophysics and Electrochemistry.

Stern–Volmer luminescence quenching experiments were carried out by monitoring the emission lifetime of **3** as a function of the concentration of **1a–e**. Luminescence decays were determined by time-correlated single photon counting on an instrument manufactured by Photochemical Research Associates (model FLI).

Electrochemistry was carried out on a cyclic voltammograph (Bioanalytical Systems, CV-27) using a glassy carbon disk working electrode, a Pt wire auxiliary electrode, and an SCE reference electrode. Cyclic voltammetry of aminoalcohols **1a–e** ( $c \approx 10$  mM) was carried out in CH<sub>3</sub>CN solution with 0.1 M tetrabutylammonium hexafluorophosphate (TBAH) as a supporting electrolyte.

Transient absorption studies were carried out on an apparatus that has been described previously.<sup>25b</sup> Excitation was effected by using the 3rd harmonic output of a Nd:YAG laser (Spectra Physics, GCR-14S), the excitation dose was 6 mJ·pulse<sup>-1</sup> (flux of 18 mJ·cm<sup>-2</sup>·pulse<sup>-1</sup>) and the pulse width was 8 ns. For transient absorption experiments the concentration of **3** was approximately 0.1 mM (absorbance at 355 nm was 0.5) and the concentrations of **1a–e** were adjusted so that the MLCT excited state of **3** was quenched with  $\approx 65\%$  efficiency. Transient absorption studies were carried out with samples contained in a flow cell to minimize the effect of sample decomposition on the kinetics. Typically a 100-mL volume of sample solution was used for each data acquisition. Temperature-dependent flash photolysis studies were carried out by using a jacketed flow cell that was maintained at constant temperature by a recirculating bath operating with a water/glycol mixture as the coolant. Activation parameters were derived from kinetic data sets comprising at least 10 rates measured at temperatures ranging from –15 to +40 °C. All Eyring plots were nicely linear.

## Fourier Transform Ion Cyclotron Resonance (FT-ICR) Studies.

FT-ICR experiments were carried out using an Ionspec data workstation equipped with a 3 T superconducting magnet. The instrument was operated in broadband mode with detection over a range of 100–400 *m/z*. The aminoalcohols were introduced via a heated solids probe to a constant background pressure of  $5 \times 10^{-8}$  Torr in the analyzer cell region. Ionization was effected by electron impact using low energies (8–16 eV) and the ions were trapped in the FT-ICR analyzer cell using a potential of +1.0 V. Short reaction delays were utilized to the limits of the instrumentation (ca. 10 ms). The excitation detection employed a standard frequency-chirp excitation. To maximize S/N ratios, 10 scans (8K data points) were obtained and co-added prior to Fourier transformations.

## Computational Methods.

Semiempirical calculations were carried out using the AM1 parameter set<sup>26a</sup> as implemented within the MOPAC 6.0 program system. Geometries of all species were optimized using the Restricted Hartree–Fock (RHF) method. In the case of open-shell systems, this leads to the “Half-Electron Configuration Interaction” (HE-CI) treatment of Dewar.<sup>26b</sup> Although the RHF/HE-CI method was exceedingly slow, it was selected over the method described by Camaioni<sup>27</sup> (UHF geometry optimization followed by a single point RHF/HE-CI calculation) because the self-consistent field (SCF) calculations did not converge under UHF with **1c**<sup>+</sup>. A similar SCF convergence problem was also encountered with **1c**<sup>+</sup> using GAMESS with UHF and the AM1 parameter set.<sup>28</sup> For all species, optimized geometries were determined by using a variety of different starting geometries in order to minimize the possibility for locating structures that correspond to a local, but not a global energy minimum. Calculations were carried out on a Sun SPARCcenter 2000 compute server and geometries were visualized by using Chem 3D on a Macintosh desktop computer.

## Results

**General Objectives and Methodology.** The principal aim of the experimental studies described herein was the follow-

(26) (a) Dewar, M. J. S.; Zoebisch, E. G.; Healy, E. F.; Stewart, J. J. P. *J. Am. Chem. Soc.* **1985**, *107*, 3902. (b) Dewar, M. J. S.; Hashmall, J. A.; Venier, C. G. *J. Am. Chem. Soc.* **1968**, *90*, 1953.

(27) Camaioni, D. M. *J. Am. Chem. Soc.* **1990**, *112*, 9475.

(28) Schmidt, M. W.; Baldrige, K. K.; Boatz, J. A.; Jensen, J. H.; Koseki, S.; Gordon, M. S.; Nguyen, K. A.; Windus, T. L.; Elbert, S. T. *QCPE Bull.* **1990**, *10*, 52.

**Table 1.** Electrochemistry of Aminoalcohols and N,N'-Dimethylaniline<sup>a</sup>

substituent	$E_p(\mathbf{1})$ V <sup>b</sup>	$dE_p/d(\log \nu)$ (mV·decade <sup>-1</sup> )	$E_{1/2}(\mathbf{2}/\mathbf{2}^{*+})$ (V) <sup>c</sup>
-OCH <sub>3</sub>	0.73	178	0.57
-CH <sub>3</sub>	0.83	73	0.73
-H	1.02	148	0.88
-Cl	1.04	121	0.91
-CN	1.31	156	1.17

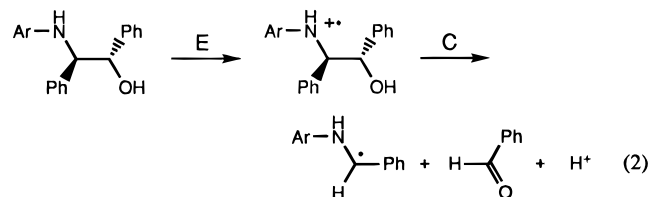
<sup>a</sup> All data for CH<sub>3</sub>CN solutions. Potentials are relative to SCE reference electrode. <sup>b</sup> Peak potential of irreversible anodic wave for first sweep at  $\nu = 100$  mV/s. <sup>c</sup> Data from ref 11c.

ing: (1) to determine the kinetics of fragmentation for the series of aminoalcohol radical cations  $\mathbf{1a-e}^{\bullet+}$  and (2) to correlate the kinetic data with the relative thermodynamic stability of the radical cations, as reflected by the thermodynamic oxidation potentials of the aminoalcohols.

Laser flash photolysis was used to determine the fragmentation kinetics of the radical cations. Thus, the transition metal complex sensitizer, [(2,2'-bipyridine)Re<sup>I</sup>(CO)<sub>3</sub>(4-benzylpyridine)]<sup>+</sup>[PF<sub>6</sub><sup>-</sup>] (**3**),<sup>29</sup> was photochemically excited with 355-nm pulses from a Nd:YAG laser. The excited state metal complex then reacts with aminoalcohols  $\mathbf{1a-e}$  by electron transfer to produce the corresponding aminoalcohol radical cations  $\mathbf{1a-e}^{\bullet+}$ , which subsequently decay by C-C bond fragmentation. In order to facilitate the flash photolysis studies the aniline chromophore was incorporated into the structure of the aminoalcohols because the aniline radical cation has a pronounced mid-visible absorption that can be easily detected by transient absorption spectroscopy.<sup>4e,23b,30</sup> It was not known at the outset of this study that  $\alpha$ -amino radicals  $\mathbf{4a-e}$  (Scheme 1), which are produced by fragmentation, exhibit pronounced absorption in the near-UV region. This serendipitous feature greatly facilitated the analysis of the transient absorption kinetics.

There are several reasons why metal complex sensitizer **3** was selected for this study. First, **3** has a long-lived metal-to-ligand charge transfer (MLCT) excited state. The MLCT state is a comparatively strong oxidant, with a reduction potential of approximately +1.22 V vs SCE.<sup>29</sup> Furthermore, previous work indicated that this sensitizer produces high yields of free radical ions as a result of excited state electron transfer reactions with amines.<sup>31</sup>

**Electrochemistry of Aminoalcohols.** Cyclic voltammograms of aminoalcohols  $\mathbf{1a-e}$  feature an irreversible anodic wave with peak potentials,  $E_p(\mathbf{1})$ , ranging from +0.7 to +1.3 V (Table 1).  $E_p(\mathbf{1})$  increases systematically with the electron withdrawing ability of the aniline substituent, consistent with assignment of the anodic wave to production of radical cations  $\mathbf{1a-e}^{\bullet+}$  via oxidation of the aniline unit. The electrochemical oxidation process is irreversible owing to the rapid chemical reaction of  $\mathbf{1a-e}^{\bullet+}$ ; in other words, the anodic oxidation is an EC process,



(29) Schanze, K. S.; MacQueen, D. B.; Perkins, T. A.; Cabana, L. A. *Coord. Chem. Rev.* **1993**, 122, 63.

(30) Shida, T. *Electronic Absorption Spectra of Radical Ions*; Elsevier: Amsterdam, 1988.

(31) Lucia, L. A.; Schanze, K. S. *Inorg. Chim. Acta* **1994**, 225, 41.

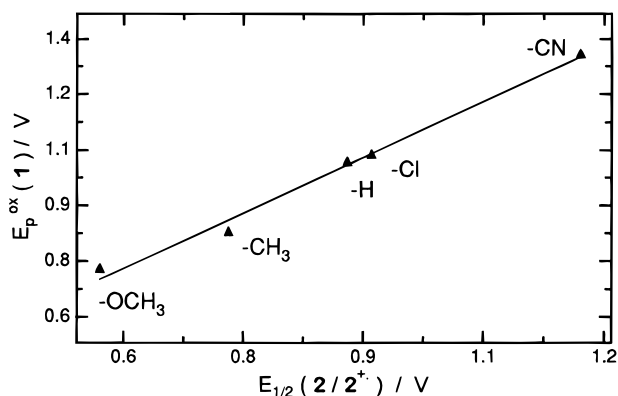


**Figure 1.** Plot of  $E_p(\mathbf{1})$  as a function of  $E_{1/2}(\mathbf{2}/\mathbf{2}^{*+})$ . Data are from Table 2 and the slope of the solid line is 1.0.

Kochi and co-workers have carefully studied the electrochemical properties of compounds that exhibit irreversible anodic waves due to an EC mechanism.<sup>32</sup> Their work demonstrates that under conditions where anodic oxidation of a series of structurally related substrates is "totally irreversible",  $E_p$  values for the series correlate well with the thermodynamic potentials ( $E^\circ$ ) for the oxidations.<sup>32a</sup> Since we were interested in establishing the relationship between  $E_p(\mathbf{1})$  and the thermodynamic potential,  $E^\circ(\mathbf{1}/\mathbf{1}^{*+})$ , experiments were carried out to demonstrate that anodic oxidation of compounds  $\mathbf{1a-e}$  is totally irreversible.

One of the principal criteria for establishing that an anodic process is totally irreversible is the observation of a sweep rate dependence for  $E_p$  in excess of 30 mV/decade.<sup>32a,33</sup> Therefore, the dependence of  $E_p(\mathbf{1})$  on the sweep rate ( $\nu$ ) for  $\mathbf{1a-e}$  was examined. Plots of  $E_p(\mathbf{1})$  vs  $\log \nu$  for  $\mathbf{1a-e}$  are linear, with slopes in most cases in excess of 100 mV/decade (Table 1), as expected if the oxidations are totally irreversible. Thus, given these relatively large  $dE_p/d\nu$  values, it is reasonable to assume that anodic oxidation of compounds  $\mathbf{1a-e}$  is totally irreversible. It follows then that  $E_p(\mathbf{1})$  should correlate linearly with  $E^\circ(\mathbf{1}/\mathbf{1}^{*+})$  for the series.<sup>32a</sup> Further support for this premise comes from correlation of  $E_p(\mathbf{1})$  values with the half-wave potentials for reversible oxidation of the series of para-substituted N,N-dimethylanilines ( $\mathbf{2a-e}$ ),  $E_{1/2}(\mathbf{2}/\mathbf{2}^{*+})$ .<sup>11c</sup> Figure 1 illustrates a plot of  $E_p(\mathbf{1})$  vs  $E_{1/2}(\mathbf{2}/\mathbf{2}^{*+})$ ; in this plot a solid line with a slope of 1.0 is drawn through the data points. Quite remarkably, this correlation indicates that the substituent effect on  $E_p(\mathbf{1})$  is exactly parallel to the substituent effect on the thermodynamic potential for the  $\mathbf{2}/\mathbf{2}^{*+}$  couple. This observation is strong evidence in support of our assertion that there is a 1:1 correlation between the substituent effects on  $E_p(\mathbf{1})$  and  $E^\circ(\mathbf{1}/\mathbf{1}^{*+})$ .

**Stern-Volmer Luminescence Quenching.** Stern-Volmer quenching experiments were carried out to determine the efficiency by which aminoalcohols  $\mathbf{1a-e}$  quench the MLCT excited state of **3**. Metal complex **3** exhibits a moderately intense MLCT emission in CH<sub>3</sub>CN ( $\lambda_{\text{max}} = 595$  nm,  $\Phi_{\text{em}} = 0.045$ ,  $\tau_{\text{em}} = 210$  ns, and  $\tau_{\text{em}}^{\text{air}} = 113$  ns).<sup>25a</sup> Stern-Volmer quenching experiments were carried out by using time-correlated single photon counting to determine the MLCT emission lifetime of an air-saturated CH<sub>3</sub>CN solution of **3** ( $\tau_{\text{em}}^{\text{air}}$ ) as a function of the concentration of  $\mathbf{1a-e}$ . Table 2 lists the second-order rate constants for MLCT emission quenching ( $k_q$ ) calculated from the slopes of the Stern-Volmer plots. The Stern-Volmer studies demonstrate that each aminoalcohol quenches the MLCT emission of **3** efficiently, presumably via electron transfer. This is expected, since given the excited state reduction potential of

(32) (a) Klingler, R. J.; Kochi, J. K. *J. Am. Chem. Soc.* **1980**, 102, 4790.

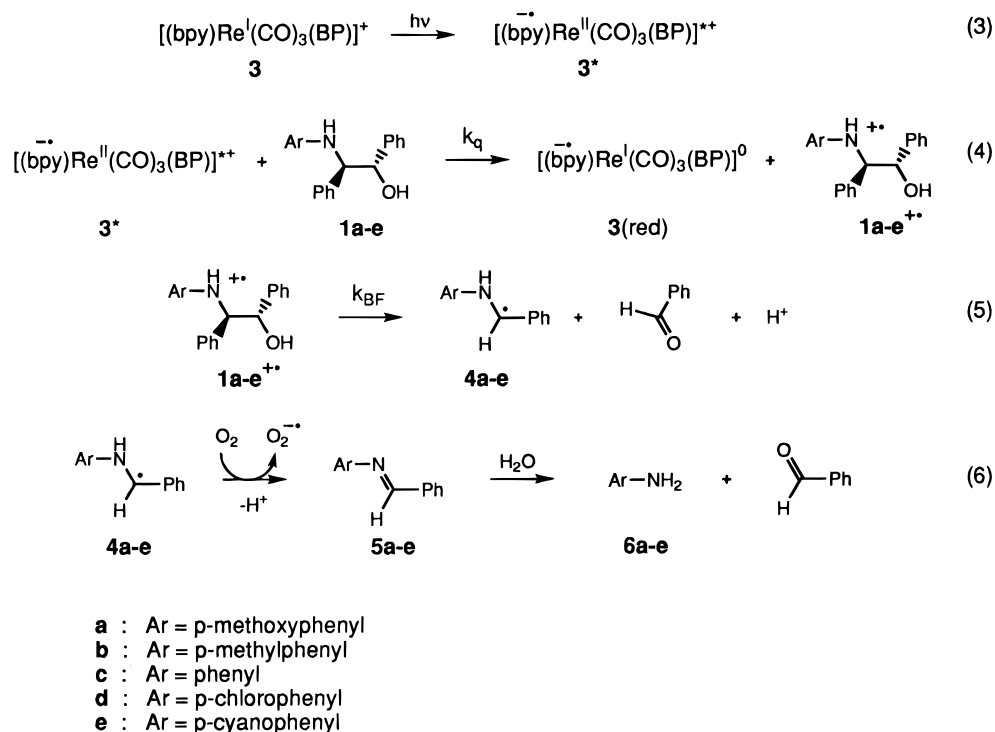
(b) Klingler, R. J.; Kochi, J. K. *J. Am. Chem. Soc.* **1982**, 104, 4186.

(33) Nicholson, R. S.; Shain, I. *Anal. Chem.* **1964**, 36, 706.

**Table 2.** Kinetic Properties of Aminoalcohols<sup>a</sup>

comp	substituent	$k_q^b$ ( $M^{-1} s^{-1}$ )	$k_{BF}(298 K)^c$ ( $s^{-1}$ )	$\Delta G_{BF}^\ddagger(298 K)$ (kcal/mol)	$\Delta H_{BF}^\ddagger$ (kcal)	$\Delta S_{BF}^\ddagger$ (cal/(mol·K))	$k_{base}^d$ ( $M^{-1} s^{-1}$ )
<b>1a</b>	–OCH <sub>3</sub>	$7.6 \times 10^9$	$3.9 \times 10^4$	11.2			$< 10^5$
<b>1b</b>	–CH <sub>3</sub>	$5.6 \times 10^9$	$2.6 \times 10^5$	10.1			$8.0 \times 10^6$
<b>1c</b>	–H	$2.3 \times 10^9$	$3.7 \times 10^5$	9.8	$7.6 \pm 1$	$-9 \pm 4$	$1.8 \times 10^8$
<b>1d</b>	–Cl	$4.2 \times 10^9$	$5.5 \times 10^5$	9.6	$3.0 \pm 1$	$-20 \pm 4$	$4.3 \times 10^8$
<b>1e</b>	–CN	$8.0 \times 10^8$	$7.4 \times 10^6$	8.1	$4.1 \pm 1$	$-12 \pm 4$	$7.5 \times 10^8$

<sup>a</sup> All data for CH<sub>3</sub>CN solutions at 25 °C. <sup>b</sup> Rate constant for Stern–Volmer quenching of luminescence of complex **3** in degassed solution. <sup>c</sup> Rate constant for C–C bond fragmentation of radical cations **1a–e**<sup>•+</sup>. Estimated error is  $\pm 10\%$ . <sup>d</sup> Rate constant for pyridine base catalyzed C–C bond fragmentation of cation radicals, **1**<sup>•+</sup>.

**Scheme 1**

the MLCT state of **3** (+1.22 V), electron transfer quenching is exothermic for most of the aminoalcohol donors.<sup>34</sup> Further evidence in support of the electron transfer quenching mechanism comes from the fact that the  $k_q$  values for **1a–e** increase as  $E_p(\mathbf{1})$  decreases.

**Steady-State Photochemical Studies.** Steady-state photochemical studies were carried out to confirm that irradiation of mixtures of metal complex **3** and aminoalcohol **1c** produces products consistent with photoinduced electron transfer and subsequent C–C bond fragmentation of radical cation **1c**<sup>•+</sup>. Thus, 3.0 mL of an air-saturated CH<sub>3</sub>CN solution of metal complex **3** ( $c = 1$  mM) and **1c** ( $c = 2.3$  mM) was irradiated at 366 nm ( $I = 6.6 \times 10^{-9}$  einsteins/s) for 10 min.<sup>35</sup> The resulting solution was analyzed by HPLC using a C<sub>18</sub> reversed phase column and a UV detector ( $\lambda = 254$  nm), and the analysis indicated that the reaction products were benzaldehyde and aniline. Quantum yield studies carried out under the conditions listed above indicated that the reaction is highly efficient; formation of benzaldehyde and disappearance of **1c** occur with quantum yields of 1.0 and 0.5, respectively.

The products and stoichiometry observed for steady-state irradiation of the mixture of **3** and **1c** are consistent with the

mechanism outlined in Scheme 1. Thus, excitation of **3** produces the metal to ligand charge transfer (MLCT) excited state, **3**<sup>\*</sup>, which is then quenched by electron transfer from **1c**. Quenching produces reduced metal complex **3** (red) and aminoalcohol radical cation **1c**<sup>•+</sup>. Radical cation **1c**<sup>•+</sup> subsequently undergoes heterolytic C–C bond fragmentation to produce  $\alpha$ -amino radical **4c** and benzaldehyde (*vide infra*). Under air-saturated conditions **4c** reacts rapidly with O<sub>2</sub> to produce imine **5c**.<sup>23c</sup> Imines of type **5c** hydrolyze under the conditions of reversed-phase HPLC analysis to produce a second equivalent of benzaldehyde and aniline (**6c**).<sup>23a</sup> Although detailed steady-state photochemical studies were not carried out on the other aminoalcohols, a consistent pattern was observed in the transient spectroscopy of each compound (*vide infra*) which strongly implies that Scheme 1 applies to all five aminoalcohols (**1a–e**).

**Laser Flash Photolysis Studies. Kinetics of C–C Bond Fragmentation of the Radical Cations.** Degassed CH<sub>3</sub>CN solutions containing metal complex **3** and aminoalcohols **1a–e** were subjected to laser flash photolysis. Excitation of solutions containing **3** and one of the aminoalcohol quenchers gave rise to moderate transient absorption throughout the near-UV and visible which persisted for greater than 100  $\mu$ s. Figure 2 illustrates the time evolution of the transient absorption of solutions containing **3** and **1c** or **1d** at times ranging from 0 to approximately 10  $\mu$ s after excitation. Time-resolved absorption

(34) The free energy for electron transfer quenching of **3**<sup>\*</sup> is given approximately by  $\Delta G_{ET} = E_p(\mathbf{1}) - 1.22$  V, where 1.22 V is the reduction potential of **3**<sup>\*</sup>.<sup>29</sup> For **1a–e**,  $\Delta G_{ET}$  ranges from  $-0.49$  (**1a**) to  $+0.1$  eV (**1e**).

(35) Only metal complex **3** absorbs light at 366 nm.

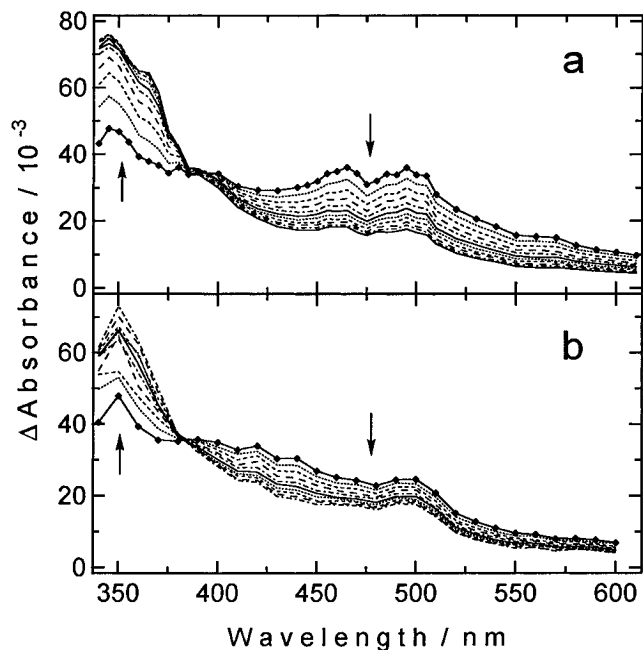


**Figure 2.** Time-resolved transient absorption difference spectra for  $\text{CH}_3\text{CN}$  solutions containing **3** ( $c = 1.2 \times 10^{-4}$  M) and either **1c** or **1d**: (a) aminoalcohol **1d** ( $c = 5 \times 10^{-3}$  M); (b) aminoalcohol **1c** ( $c = 5 \times 10^{-3}$  M). Delay times range from 0 to 4  $\mu\text{s}$  following excitation with a pulse from a Nd:YAG laser (355 nm, 6 mJ/pulse, 8 ns fwhm). The solid line marked with polygons is the spectrum immediately after laser pulse and arrows indicate the direction of change in absorbance with increasing delay time.

spectra of **3** with the other aminoalcohols were similar. For each aminoalcohol, at early delay times the difference spectra display absorption throughout the near-UV and visible region; however, an absorption band in the 450–500-nm region is clearly discernible. This mid-visible absorption is clearly delineated for aminoalcohol **1d** (Figure 2a) where band maxima appear at 465 and 495 nm. This mid-visible absorption is attributed to the aniline radical cation chromophore (**1a-e**<sup>+</sup>, Scheme 1), which is produced by photoinduced electron transfer.<sup>4e,23b,30</sup> Figure 2 also reveals that the difference spectra evolve during the 0–10  $\mu\text{s}$  time domain and the evolution is characterized by the following: (1) a decrease in the absorption of the aniline radical cation chromophore in the 450–500-nm region and (2) appearance of a strong absorption band at 360–370 nm in the near-UV. The spectral evolution is attributed to heterolytic C–C bond fragmentation of radical cations **1a-e**<sup>+</sup> to produce benzaldehyde and  $\alpha$ -amino radicals, **4a-e** (eq 5, Scheme 1). The absorption band that appears at 360–370 nm concomitant to disappearance of the aniline radical cation absorption is attributed to radicals **4a-e**. The large absorptivity and low energy of this absorption band is consistent with the highly delocalized electronic structure **4a-e**, and the spectral assignment is also supported by the observation of similar absorption features in structurally similar radicals.<sup>36</sup>

Global kinetic analysis<sup>38</sup> was applied to the multiwavelength transient absorption data for aminoalcohols **1a-e** to determine the rates of C–C bond fragmentation for the corresponding radical cations ( $k_{\text{BF}}$ , eq 5, Scheme 1). For each aminoalcohol,

(36) The (*N*-methylamino)methyl radical (e.g., the conjugate base of **2c**<sup>+</sup>) has a strong absorption band at 330 nm.<sup>37</sup> Also,  $\alpha$ -amino radicals produced by C–C bond fragmentation of 1,2-diaminoethane radical cations generally exhibit strong absorption in the 340–370-nm region.<sup>23</sup>

(37) Holcman, J.; Sehested, K. *J. Phys. Chem.* **1977**, *81*, 1963.

(38) (a) SPECTFIT (version 2.10), Spectrum Software Associates: Chapel Hill, NC, 1996. (b) Stultz, L. K.; Binstead, R. A.; Reynolds, M. S.; Meyer, T. J. *J. Am. Chem. Soc.* **1995**, *117*, 2520.

the kinetics of the transient absorption spectral evolution were simulated very well over the entire spectral range from 330 to 600 nm by using a first-order kinetic model.<sup>39</sup> The first-order rate constants derived from the global analysis are summarized in Table 2. Inspection of these data reveals that the bond fragmentation rate increases systematically with  $E_p(\mathbf{1})$ , which indicates that  $k_{\text{BF}}$  increases as the stability of the radical cation decreases. The implications of the correlation between  $k_{\text{BF}}$  and  $E_p(\mathbf{1})$  are discussed in detail below.

Activation parameters for bond fragmentation ( $\Delta H_{\text{BF}}^\ddagger$  and  $\Delta S_{\text{BF}}^\ddagger$ ) in **1c-e**<sup>+</sup> were determined from Eyring analysis of  $k_{\text{BF}}$  over the temperature range from –10 to +35 °C (Table 2). The temperature-dependent kinetic data reveal that bond fragmentation in the radical cations is characterized by comparatively low activation enthalpies and negative activation entropies.

**Base-Catalyzed C–C Bond Fragmentation.** Previous studies with **3** and **1c** revealed that addition of pyridine or substituted pyridines accelerates the rate of C–C bond fragmentation of **1c**<sup>+</sup>.<sup>23b</sup> Kinetic studies of **1c** as a function of pyridine concentration demonstrated that the rate of fragmentation in the presence of pyridine ( $k_{\text{obs}}$ ) followed a linear relationship of the form

$$k_{\text{obs}} = k_{\text{BF}} + k_{\text{base}}[\text{pyridine}] \quad (7)$$

where  $k_{\text{base}}$  is the second-order rate constant for the base-catalyzed reaction pathway. Similarly,  $k_{\text{base}}$  was determined for **1c**<sup>+</sup> with a series of substituted pyridines,<sup>40</sup> and a correlation of  $k_{\text{base}}$  with  $\text{p}K_{\text{a}}$  for the series of pyridines yielded a Brønsted coefficient,  $\beta = 0.62$ .<sup>23b</sup> Finally,  $k_{\text{base}}$  for reaction of **1c-OD** with pyridine yielded a deuterium isotope effect,  $k_{\text{base}}^{\text{H}}/k_{\text{base}}^{\text{D}} = 2.0$ .

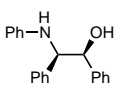
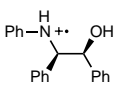
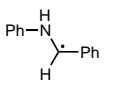
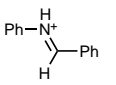
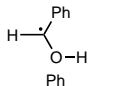
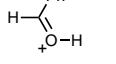
In the present study, the effect of pyridine on the rates of C–C bond fragmentation in **1a**<sup>+</sup>, **1b**<sup>+</sup>, **1d**<sup>+</sup>, and **1e**<sup>+</sup> was determined. The rates of fragmentation were measured as a function of [pyridine], and  $k_{\text{base}}$  was determined from linear correlations of  $k_{\text{obs}}$  vs [pyridine] according to eq 7. As noted for **1c**<sup>+</sup>, pyridine accelerates the rate of fragmentation of **1b**<sup>+</sup>, **1d**<sup>+</sup>, and **1e**<sup>+</sup>, and  $k_{\text{base}}$  values for these radical cations are listed in Table 2. Rate acceleration was not observed for fragmentation of **1a**<sup>+</sup> for [pyridine]  $\leq 0.1$  M, which indicates that  $k_{\text{base}} \leq 10^5 \text{ M}^{-1} \text{ s}^{-1}$  for this radical cation. Inspection of the data in Table 2 reveals that  $k_{\text{base}}$  increases with  $E_p(\mathbf{1})$  and the significance of this correlation is discussed below.

**Gas-Phase Bond Fragmentation Studies.** Fourier Transform Ion Cyclotron Resonance (FT-ICR) studies were carried out to determine the fragmentation pathways for radical cations **1a-e**<sup>+</sup> in the gas phase. It was also hoped that it might be possible to monitor the kinetics of the gas-phase fragmentation reactions. Aminoalcohols **1a-e** were introduced into the FT-ICR cell via a heated solids probe and the radical cations were generated by electron impact ionization. The lowest possible electron energy was used in order to increase the probability of observing the parent radical cations (8–16 eV was typically required). Despite this effort, for each aminoalcohol only fragment ions were detected, even at the earliest accessible delay times. As a result, it was not possible to monitor the gas-phase fragmentation kinetics. For each aminoalcohol, the most prominent ion peak in the mass spectrum corresponded to iminium ion **7**, which implies that the dominant fragmentation

(39) The kinetics of the spectral evolution that is attributed to C–C bond fragmentation of cation radicals **1a-e**<sup>+</sup> is independent of the laser excitation power. This is consistent with the fact that C–C bond fragmentation is a first-order process.

(40) The series of pyridines included 4-chloropyridine, pyridine, 4-methylpyridine, and 3,4-dimethylpyridine.<sup>23b</sup>

**Table 3.** AM1 Calculated Heats of Formation

structure	acronym	conformation	$\Delta H_f^a$ (kcal/mol)	$\Delta H_{\text{hom}}^b$ (kcal/mol)	$\Delta H_{\text{het}}^c$ (kcal/mol)
	<b>1c</b>	C1 and C2 phenyls gauched	31.6	41	
	<b>1c<sup>+</sup></b>	C <sub>1</sub> and C <sub>2</sub> phenyls gauche <sup>d</sup>	204.4	10	29
	<b>4c</b>	phenyls anti	73.9		
	<b>7c</b>	phenyls trans	215.4		
	<b>8</b>	phenyl and H syn	-1.4		
	<b>9</b>	phenyl and H syn	159.7		

<sup>a</sup> Calculated values obtained by use of AM1 (MOPAC 6.0). Even electron species computed by using RHF and odd electron species calculated by using RHF/HE-Cl. <sup>b</sup> AM1 calculated enthalpy for C–C bond homolysis. <sup>c</sup> AM1 calculated enthalpy for C–C bond heterolysis. <sup>d</sup> See Figure 3 for structures.

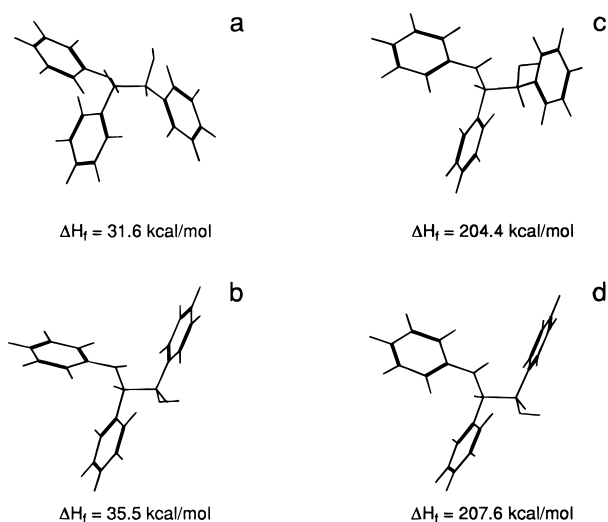


**Figure 3.** Vector plots of RHF or RHF/HE-Cl energy minimized structures: (a) **1c**, lowest energy conformation, C<sub>1</sub> and C<sub>2</sub> phenyls gauche; (b) **1c**, local energy minimum, C<sub>1</sub> and C<sub>2</sub> phenyls anti; (c) **1c<sup>+</sup>**, lowest energy conformation, C<sub>1</sub> and C<sub>2</sub> phenyls gauche; and (d) **1c<sup>+</sup>**, local energy minimum, C<sub>1</sub> and C<sub>2</sub> phenyls anti.

pathway for radical cations **1a–e<sup>+</sup>** in the gas phase is homolytic C–C bond fragmentation (see eq 9 in Scheme 2).

**Semiempirical Calculations.** Semiempirical calculations were carried out using the AM1 parameter set within MOPAC 6.0 to provide insight concerning C–C bond fragmentation in **1c<sup>+</sup>**. Computational methods are described in the Experimental Section. Table 3 contains a listing of RHF or RHF/HE-Cl calculated  $\Delta H_f$  values for **1c**, the corresponding radical cation **1c<sup>+</sup>**, and several reactive intermediates that are produced by either heterolytic or homolytic bond scission of the aminoalcohol neutral or radical cation. Where ever comparisons can be made, our calculated energies compare favorably with results previously reported by Camaioni.<sup>27</sup> An interesting feature that emerges from the AM1 calculations is that in the energy-minimized structures of **1c** and **1c<sup>+</sup>** (Figure 3), the aniline nitrogen and hydroxy oxygen are gauche and the C<sub>1</sub> and C<sub>2</sub> phenyl groups are gauche. For **1c** and **1c<sup>+</sup>** the energies of these conformers lie approximately 4 kcal/mol lower than the energies of conformations in which the nitrogen and oxygen are anti and

the C<sub>1</sub> and C<sub>2</sub> phenyl groups are anti (Figure 3). Thus, the calculations suggest that the steric interaction between the N-phenyl and C<sub>1</sub> phenyl is larger than that between the C<sub>1</sub> and C<sub>2</sub> phenyls. This observation is significant, because it has been previously suggested that in the preferred conformation of the transition state for C–C bond fragmentation in **1c<sup>+</sup>**, the aniline nitrogen and hydroxy oxygen are anti and the C<sub>1</sub> and C<sub>2</sub> phenyl groups are anti.<sup>24b,e</sup> Therefore, if the calculations are correct, they imply that part of the activation energy for bond fragmentation of **1c<sup>+</sup>** may be due to the requirement for endothermic conformational rearrangement to the anti conformer.

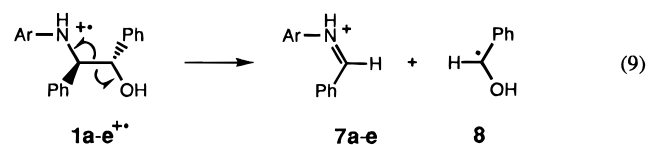
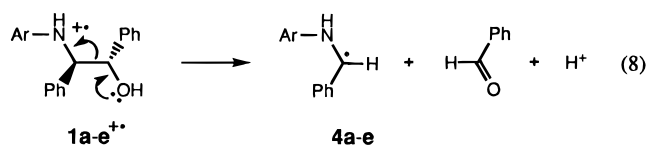
The  $\Delta H_f$  data can be used to calculate enthalpies for homolysis of the C<sub>1</sub>–C<sub>2</sub> bond in **1c** ( $\Delta H_{\text{hom}}$ ), and for homolysis and heterolysis ( $\Delta H_{\text{het}}$ ) of the C<sub>1</sub>–C<sub>2</sub> bond in **1c<sup>+</sup>** (Table 3). First,  $\Delta H_{\text{hom}}$  calculated for **1c** (41 kcal/mol) is in reasonable agreement with AM1 calculated<sup>27</sup> and experimental<sup>6c</sup>  $\Delta H_{\text{hom}}$  values for other 1,2-substituted diphenylethanes. Second, for radical cation **1c<sup>+</sup>** two bond scission modes can be considered (eqs 8 and 9, Scheme 2). The AM1 calculations imply that in the gas phase the thermodynamically preferred mode of fragmentation is bond homolysis, which has  $\Delta H_{\text{hom}} = 10$  kcal/mol; further, this pathway is preferred over heterolysis by approximately 20 kcal/mol ( $\Delta H_{\text{het}} = 29$  kcal/mol).

## Discussion

**Mechanism and Thermodynamics of C–C Bond Fragmentation.** As implied above, carbon–carbon bond fragmentation in **1a–e<sup>+</sup>** must occur either via heterolytic or homolytic scission of the C–C  $\sigma$  bond (eqs 8 and 9, respectively, Scheme 2). These two pathways are distinguishable based on the reactive intermediates that are formed by the fragmentation:  $\alpha$ -amino radicals **4a–e** are produced by bond heterolysis while the  $\alpha$ -hydroxy benzyl radical (**8**) and iminium ions **7a–e** are produced by bond homolysis.

The experimental data indicate that in CH<sub>3</sub>CN solution **1a–e<sup>+</sup>** fragment via heterolysis. Transient absorption spectroscopy reveals that a species with a strong near-UV absorption ( $\lambda_{\text{max}} \approx 360$  nm) is produced by fragmentation; this species cannot be ketyl radical **8**, which has its most prominent absorption band below 300 nm.<sup>41</sup> Furthermore, observation of base catalysis

## Scheme 2



for fragmentation points to involvement of proton loss in the rate determining step. Both of these lines of evidence support the premise that heterolytic fragmentation occurs in solution. By contrast, the FT-ICR data clearly indicate that in the gas phase, radical cations **1a-e<sup>+</sup>** fragment homolytically. This is indicated by the observation of iminium ions **7a-e** as the predominant charged species produced when **1a-e** are ionized in the gas phase.<sup>42</sup>

Consideration of the thermodynamics for C–C bond fragmentation in **1a-e<sup>+</sup>** provides a rationale for the difference in bond fragmentation modes observed in solution and the gas phase. Figure 4 outlines three thermodynamic cycles that can be applied to calculate the free energy for C–C bond fragmentation in **1a-e<sup>+</sup>** ( $\Delta G_4$ ), and Table 4 provides a tabular summary of the necessary equations and the calculated thermodynamic quantities.<sup>15</sup> Three modes of bond fragmentation are considered in this diagram: (a) homolytic fission ( $\Delta G_{4a}$ ); (b) heterolytic fission without loss of a proton from the benzaldehyde oxygen ( $\Delta G_{4b}$ ); and (c) heterolytic fission with concomitant loss of a proton from the benzaldehyde oxygen ( $\Delta G_{4c}$ ). Three free energies are required for estimation of  $\Delta G_4$  (Table 4): the free energy for C–C bond homolysis in the neutrals **1a-e** ( $\Delta G_1$ ); the free energy for electrochemical reduction of **1a-e<sup>+</sup>** relative to the SCE ( $\Delta G_2$ ); and the free energy for electrochemical reduction of one of the products of bond fission relative to the SCE ( $\Delta G_{3a}$ ,  $\Delta G_{3b}$  or  $\Delta G_{3c}$ ).

Sufficient experimental data are available in the literature or from the present study to evaluate each of the required free energies. Table 4 provides a tabular summary of how each thermodynamic parameter was obtained or estimated. First, an estimate for the free energy of homolysis of **1c** ( $\Delta G_1$ ) was arrived at by taking the literature bond enthalpy of 2-aminoethanol ( $\Delta H = 80$  kcal/mol), subtracting the steric and electronic effect typical of 1,2-diphenyl substitution on the C–C bond enthalpy of ethane ( $\Delta H \approx 22$  kcal/mol), and using an entropy value which is typical for bond homolysis of substituted ethanes ( $\Delta S \approx 36$  cal/(mol·K)).<sup>43</sup> These values lead to an estimate of  $\Delta G_1 = 47$  kcal/mol, which is in accord with experimentally determined free energies for bond homolysis of substituted 1,2-diphenylethanes in which the C–C bond is weakened by steric and electronic effects (30–43 kcal/mol).<sup>6c</sup> Second,  $\Delta G_2$  was estimated based on  $E_p(\mathbf{1c})$ , which provides a value which is intermediate for the series **1a-e**. Finally,  $\Delta G_{3a}$ ,  $\Delta G_{3b}$ , and  $\Delta G_{3c}$  were derived from electrochemical data as follows:  $\Delta G_{3a}$  from the reduction potential of iminium ion **7**,<sup>44a</sup>  $\Delta G_{3b}$  from the reduction potential of benzaldehyde ( $E_p = -1.55$  V),<sup>44b</sup> the  $pK_a$

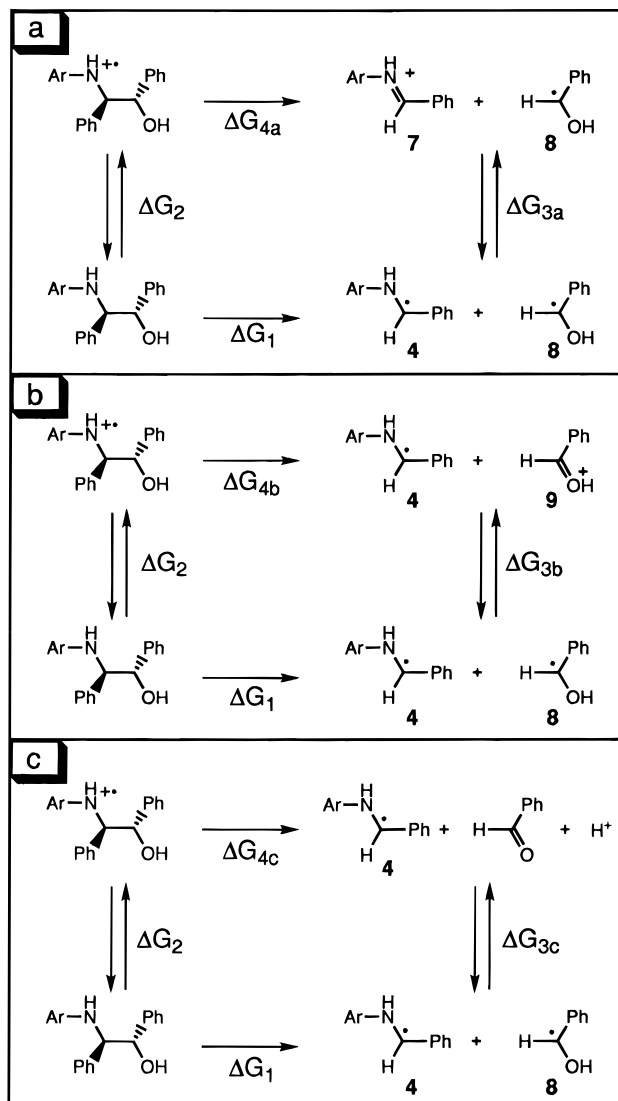


**Figure 4.** Thermodynamic cycles for calculation of free energy for C–C bond fragmentation in aminoalcohol radical cations.

**Table 4.** Thermodynamics of Bond Fragmentation Estimated by Thermochemical Cycles<sup>a</sup>

parameter	value (kcal·mol <sup>-1</sup> ) <sup>b</sup>	method of calculation
$\Delta G_1$	+47	estimated as described in text
$\Delta G_2$	-23	$\Delta G_2 = -FE_p(\mathbf{1c})$
$\Delta G_{3a}$	+19	$\Delta G_{3a} = -FE_{1/2}(\mathbf{7/4})$ , where $E_{1/2}(\mathbf{7/4}) = -0.84$ V <sup>44a</sup>
$\Delta G_{3b}$	+15	$\Delta G_{3b} = -FE_{1/2}(\mathbf{9/8})$ , where $E_{1/2}(\mathbf{9/8}) =$ -66 V calculated described in text
$\Delta G_{3c}$	+25	$\Delta G_{3c}$ calculated as described in text
$\Delta G_{4a}$	+5	$\Delta G_{4a} = \Delta G_1 + \Delta G_2 - \Delta G_{3a}$
$\Delta G_{4b}$	+9	$\Delta G_{4b} = \Delta G_1 + \Delta G_2 - \Delta G_{3b}$
$\Delta G_{4c}$	-1	$\Delta G_{4c} = \Delta G_1 + \Delta G_2 - \Delta G_{3c}$

<sup>a</sup> Refer to Figure 4 for definition of the thermodynamic quantities.  $F$  is the Faraday constant (23.06 kcal·mol<sup>-1</sup>·eV<sup>-1</sup>). <sup>b</sup> Estimated errors in  $\Delta G_1$ – $\Delta G_3$  are  $\pm 10\%$ .

of the  $\alpha$ -hydroxybenzyl radical (structure **8**,  $pK_a = 8.1$ ),<sup>44b</sup> and the  $pK_a$  of the  $\alpha$ -hydroxybenzyl cation (structure **9**,  $pK_a = -7$ ),<sup>45</sup> and  $\Delta G_{3c}$  from the reduction potential of benzaldehyde and the  $pK_a$  of the  $\alpha$ -hydroxybenzyl radical.<sup>46</sup>

Some very interesting features are apparent from consideration of the  $\Delta G_4$  values (Table 4) which are calculated for the

(45) March, *J. Advanced Organic Chemistry*, 4th ed.; Wiley-Interscience: New York, 1992; p 250.

(42) DeJohgh, D. C.; Liu, D. C. K.; Leclair-Lanteigne, P.; Gravel, D. *Can. J. Chem.* **1975**, *53*, 3175.

(43) McMillin, D. F.; Golden, D. M. *Annu. Rev. Phys. Chem.* **1982**, *33*, 493.

(44) (a) Andrieux, C. P.; Saveant, J.-M. *J. Electroanal. Chem.* **1970**, *26*, 223. (b) Andrieux, C. P.; Grzeszczuk, M.; Saveant, J.-M. *J. Am. Chem. Soc.* **1991**, *113*, 8811.



pathways in Figures 4a–c. First, all of the  $\Delta G_4^\ddagger$ 's are  $<10$  kcal/mol, indicating that regardless of mechanism, C–C bond scission in  $\mathbf{1a-e}^{\bullet+}$  is weakly endothermic at most. Thus, single electron oxidation of the aminoalcohols significantly activates the C–C bond toward scission. Even more interesting is the relationship between the  $\Delta G_4^\ddagger$ 's that are calculated for the three fragmentation pathways. The pathways in Figures 4a and 4b involve bond scission without concomitant loss of the proton from the carbonyl oxygen. Under these circumstances, homolysis (pathway a,  $\Delta G_{4a}^\ddagger$ ) is favored by ca. 4 kcal/mol over heterolysis (pathway b,  $\Delta G_{4b}^\ddagger$ ). However, the calculations also show that when heterolytic C–C bond scission occurs *with concomitant loss of a proton* (pathway c,  $\Delta G_{4c}^\ddagger$ ), this pathway is thermodynamically preferred over homolysis (pathway a) by more than 5 kcal/mol.

With this thermodynamic information at hand, it is now possible to rationalize why C–C bond scission in  $\mathbf{1a-e}^{\bullet+}$  occurs via homolysis in the gas phase and via heterolysis in solution. In the gas phase, there are no readily available proton acceptors. Under this circumstance iminium ions  $\mathbf{7a-e}$  are the best electrofugal groups and bond homolysis predominates. By contrast, in solution the solvent and/or added base facilitates heterolytic fragmentation by accepting the proton from the incipient carbonyl oxygen. Under this circumstance the benzaldehyde fragment is the best electrofugal group and bond heterolysis predominates. This analysis provides a good indication that even in the absence of a basic catalyst (such as pyridine), in solution C–C bond scission in  $\mathbf{1a-e}^{\bullet+}$  occurs with concomitant loss of the proton from the incipient carbonyl oxygen.

We now briefly compare the results of the thermodynamic cycle calculations, which are based upon experimental data, with those of the AM1 calculations. The RHF calculated bond homolysis enthalpy for neutral aminoalcohol  $\mathbf{1c}$  ( $\Delta H_{\text{hom}} = 41$  kcal/mol) is lower than expected based on the estimate of  $\Delta G_1$  (47 kcal/mol), which was arrived at by the thermodynamic cycle calculation. Camaioni has noted that AM1 consistently underestimates  $\Delta H_f$  values for carbon-based radicals; furthermore, his results indicate that the degree of underestimation is larger when the carbon radical bears an  $\alpha$  heteroatom substituent.<sup>27</sup> Since the AM1-calculated  $\Delta H_{\text{hom}}$  for  $\mathbf{1c}$  relies on  $\Delta H_f$  values for benzyl radicals which feature an  $\alpha$  heteroatom (e.g.,  $\mathbf{4c}$  and  $\mathbf{8}$ ), it is likely that our AM1-calculated  $\Delta H_{\text{hom}}$  is lower than the true value because of underestimation of the  $\Delta H_f$  values for these two radicals. Thus, we believe that the free energy for bond homolysis which is based on the thermodynamic cycle calculation (e.g.,  $\Delta G_1$ ) is probably a better estimate for the bond energy of aminoalcohol  $\mathbf{1c}$ .

Another interesting feature that emerges from the calculations is that AM1 correctly predicts that bond homolysis is the preferred pathway for the gas-phase fragmentation of  $\mathbf{1c}^{\bullet+}$ . However, a disparity between the AM1 calculations and those based on thermodynamic cycles is that AM1 predicts that the pathway in Figure 4a is favored over that in Figure 4b by over 20 kcal/mol, while the thermodynamic cycle suggests only a 4 kcal/mol difference. It is important to note that the AM1 calculations refer to gas-phase processes while the thermodynamic cycle calculations are based primarily on free energies for the solution-phase counterparts. Thus, it is possible that the large difference in the enthalpies for the two homolysis pathways (e.g., Figures 4a and 4b) in the gas phase is offset partly in the solution-phase counterparts by solvation effects.

(46) In the redox process which defines  $\Delta G_{3c}$ ,  $\text{PhCHO} + \text{H}^+ + \text{e}^- \rightarrow \text{PhCHOH}^\bullet$ , " $\text{H}^+$ " refers to  $\text{H}^+$  in the standard state (e.g., aqueous  $\text{H}^+$ , pH 0).

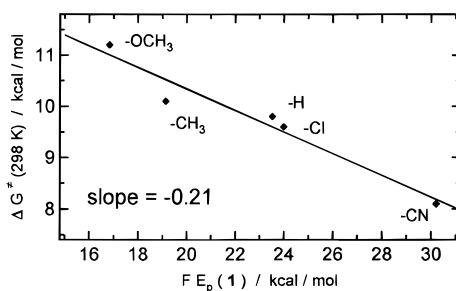


Figure 5. Linear free energy correlation for bond fragmentation of radical cations  $\mathbf{1a-e}^{\bullet+}$ .

Specifically, the observed difference in the thermodynamics of the gas-phase and solution-phase reactions can be explained if the solvation energy of the  $\alpha$ -hydroxybenzyl cation ( $\mathbf{9}$ ) is greater than that of the iminium ion ( $\mathbf{7}$ ).

**Kinetics of Radical Cation Bond Fragmentation. Correlations and Mechanistic Implications.** As noted above, the rates of C–C bond fragmentation in  $\mathbf{1a-e}^{\bullet+}$  increase with  $E_p(\mathbf{1})$ . The strong correlation between  $k_{\text{BF}}$  and  $E_p(\mathbf{1})$  is highlighted by a plot of the free energy of activation for bond fragmentation ( $\Delta G_{\text{BF}}^\ddagger$ ) vs  $FE_p(\mathbf{1})$ , where  $F$  is the Faraday constant (Figure 5). The solid line in the correlation was generated by linear least-squares regression ( $r = 0.9722$ , slope =  $-0.21$ ). Since both parameters used in the free energy correlation are expressed in units of kilocalories per mole, the slope of the line provides a direct measure of the effect of radical cation stability (as reflected by  $E_p(\mathbf{1})$ ) on  $\Delta G_{\text{BF}}^\ddagger$ . Thus, the relatively small slope of the correlation indicates that the effects of the para substituent on the energies of the reactant (radical cation) and transition state are similar. This is consistent with the reaction having an early transition state, as expected if fragmentation is weakly endothermic or exothermic.<sup>47</sup>

Previous work indicates that remote substituents have little effect on radical stability.<sup>48,49</sup> On this basis, we suggest that the para substituents have little effect on the energy of the  $\alpha$ -amino radicals ( $\mathbf{4a-e}$ ) produced by heterolytic bond fragmentation of  $\mathbf{1a-e}^{\bullet+}$ . Thus, the substituent effect on the rate of bond scission is caused by the effect of the substituent on the energy of the radical cation reactant and the transition state. Furthermore, if the substituents have little influence on the energy of  $\mathbf{4a-e}$ , then the correlation of  $\Delta G_{\text{BF}}^\ddagger$  with  $FE_p(\mathbf{1})$  can be viewed as a free energy correlation, where the  $x$ -coordinate is directly proportional to the free energy of bond fragmentation,  $\Delta G_{\text{BF}}^\circ$  (e.g.,  $FE_p(\mathbf{1}) = \Delta G_{\text{BF}}^\circ + \text{constant}$ ).

Maslak has demonstrated that the free energy dependence for the rate of bond scission in a series of benzylic radical ions correlates with Marcus theory.<sup>6d</sup> If the data for the aminoalcohols is considered within the framework of a similar analysis, then the observed slope of the correlation of  $\Delta G_{\text{BF}}^\ddagger$  vs  $\Delta G_{\text{BF}}^\circ$  (Figure 5, slope =  $-0.21$ ) implies that bond fragmentation of  $\mathbf{1a-e}^{\bullet+}$  is weakly exothermic. This conclusion follows from Marcus theory, which indicates that the slope of a plot of  $\Delta G^\ddagger$  vs  $\Delta G^\circ$  for a reaction with  $\Delta G^\circ < 0$  is less than 0.5.<sup>50</sup>

The bond fragmentation kinetics of  $\mathbf{1c-e}^{\bullet+}$  are characterized by comparatively low activation enthalpies and moderately large negative activation entropies. Similar activation parameters were observed by Maslak and co-workers in their recent studies of C–C bond fragmentation in sterically congested 1,2-

(47) Hammond, G. S. *J. Am. Chem. Soc.* **1955**, *77*, 334.

(48) Dust, J. M.; Arnold, D. R. *J. Am. Chem. Soc.* **1983**, *105*, 1221.

(49) Bordwell, F. G.; Bausch, M. J. *J. Am. Chem. Soc.* **1986**, *108*, 2473.

(50) For examples of the application of this concept see: (a) Fukuzumi, S.; Wong, C. L.; Kochi, J. K. *J. Am. Chem. Soc.* **1980**, *102*, 2928. (b) Bock, C. R.; Connor, J. A.; Guitierrez, A. R.; Meyer, T. J.; Whitten, D. G.; Sullivan, B. P.; Nagle, J. K. *J. Am. Chem. Soc.* **1979**, *101*, 4815.

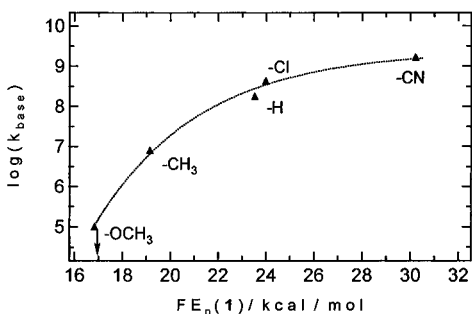


**Figure 6.** Plot of  $\log(k_{\text{base}})$  for aminoalcohol radical cations as a function of  $FE_p(\mathbf{1})$  ( $F$  is faraday constant,  $23.06 \text{ kcal}\cdot\text{V}^{-1}$ ). The line is simply a smooth curve drawn through the data points.

diphenylethane radical cations.<sup>6c</sup> Importantly, the consistency of our findings with those of Maslak clearly indicates that an unfavorable activation entropy is typical for bond scission of radical cations in moderately polar solvents. The large negative  $\Delta S^\ddagger$  values that are observed for the radical cation fragmentations likely have their origin in the interactions of solvent molecules with the radical cation reactant and the transition state for fragmentation. Further, it is possible that part of the unfavorable activation entropy component may be related to stereoelectronic demands of the transition state.<sup>8d,27</sup>

**Mechanism of Base-Catalyzed Fragmentation.** The observation of base catalysis for bond fragmentation in  $\mathbf{1a-e}^{\bullet+}$  indicates that proton loss is involved in the rate determining step for fragmentation, at least in the presence of an added base. Two mechanisms can be considered for the base-catalyzed fragmentation reaction. The first, which corresponds to an E2 elimination, involves concerted deprotonation at the hydroxyl group and C–C bond fragmentation. In this case, proton transfer is rate determining and the observed second-order rate ( $k_{\text{base}}$ ) corresponds to the deprotonation rate. The second mechanism corresponds to an E1cB elimination and involves initial deprotonation at the hydroxyl group to form the conjugate base of the aminoalcohol radical cation. Deprotonation is then followed by C–C bond fragmentation in the conjugate base of the radical cation. In the E1cB mechanism, the rate for disappearance of the radical cation is first order in base, but the relationship of the observed rate to the microscopic rate constants depends upon the relative rates of the individual steps.

Fragmentation of  $\mathbf{1b-e}^{\bullet+}$  is catalyzed by pyridine base and the observed second-order rate constants for fragmentation ( $k_{\text{base}}$ ) increase with  $E_p(\mathbf{1})$ . Figure 6 illustrates a plot of  $\log(k_{\text{base}})$  as a function of  $FE_p(\mathbf{1})$ . This plot indicates that  $k_{\text{base}}$  varies only weakly with  $E_p(\mathbf{1})$  for  $\mathbf{1c-d}^{\bullet+}$ , but becomes significantly slower for  $\mathbf{1b}^{\bullet+}$  and immeasurably slow for  $\mathbf{1a}^{\bullet+}$ . If the mechanism for the base-catalyzed fragmentation reaction is the same among the entire series of radical cations, the correlation of  $\log(k_{\text{base}})$  vs  $E_p(\mathbf{1})$  is expected to be linear;<sup>51</sup> thus, the nonlinearity of the correlation suggests that the mechanism for base catalysis may change as a function of  $E_p(\mathbf{1})$ .

As noted above, if deprotonation and fragmentation are concerted, then  $k_{\text{base}}$  corresponds to the rate of deprotonation of the radical cation. Therefore, if the reaction is concerted, variation of  $k_{\text{base}}$  with  $E_p(\mathbf{1})$  reveals the effect of radical cation stability on the thermodynamic acidity (as reflected by the rate of deprotonation). Since deprotonation of the aminoalcohol radical cations presumably occurs at the hydroxy group, we expect the remote para substituent to have only a modest effect on the thermodynamic and kinetic acidity. This is consistent with the experimental observations for radical cations  $\mathbf{1c-e}^{\bullet+}$  (e.g., for these radical cations the substituent has a comparatively weak effect on  $k_{\text{base}}$ ). On this basis we suggest that base-catalyzed fragmentation in  $\mathbf{1c-e}^{\bullet+}$  occurs via an E2-like concerted mechanism. By contrast,  $k_{\text{base}}$  decreases sharply with  $E_p(\mathbf{1})$  for the radical cations derived from  $\mathbf{1a}$  and  $\mathbf{1b}$ . While the underlying basis for this effect is unclear, it is possible that for these radical cations base catalysis occurs via an E1cB mechanism, or by an entirely different mechanism involving deprotonation at a different position.

## Summary and Conclusions

The kinetics and mechanism of bond fragmentation in radical cations derived from aminoalcohols  $\mathbf{1a-e}$  have been examined. The rates of bond fragmentation in the radical cations in  $\text{CH}_3\text{CN}$  solution were determined by laser flash photolysis. A correlation of the observed rates with the peak potentials for anodic oxidation of the neutral aminoalcohols indicates that the rate of C–C bond fragmentation increases, albeit weakly, with decreasing stability of the radical cations. Prominent features in the transient absorption spectra of the reactive intermediates produced by the reaction indicate that (in solution) heterolytic bond fragmentation occurs. By contrast, FT-ICR studies of the products arising from fragmentation of  $\mathbf{1a-e}^{\bullet+}$  indicate that, in the gas phase, homolytic C–C bond fragmentation predominates. AM1-calculated enthalpies for bond homolysis and heterolysis of  $\mathbf{1c}^{\bullet+}$  reveal that C–C bond homolysis is thermodynamically preferred over heterolysis by 20 kcal/mol, consistent with the gas-phase experimental results. By contrast, free energies for C–C bond homolysis and heterolysis estimated from (solution phase) thermodynamic data indicate that in solution, heterolytic bond fragmentation with concurrent deprotonation is the thermodynamically preferred reaction pathway, again consistent with the experimental data.

**Acknowledgment.** We gratefully acknowledge the National Science Foundation (Grant No. CHE-9401620) for support of this work.

JA960378Q

(51) (a) Bunting, J. W.; Stefanidis, D. *J. Am. Chem. Soc.* **1988**, *110*, 4008. (b) Bunting, J. W.; Kanter, J. P. *J. Am. Chem. Soc.* **1991**, *113*, 6950.